JGR Atmospheres

RESEARCH ARTICLE
10.1029/2024JD041455

How Do Schumann Resonance Frequency Changes in the Vertical Electric Field Component Reflect Global Lightning Dynamics at Different Time Scales?

G. Sátori[1], T. Bozóki[1,2], E. Williams[3,4], E. Prácser[1], H. Mátyás[1,5], R. I. Albrecht[6], and R. P. Beltran[6]

[1]HUN-REN Institute of Earth Physics and Space Science, Sopron, Hungary, [2]Department of Geophysics and Space Science, Institute of Geography and Earth Sciences, ELTE Eötvös Loránd University, Budapest, Hungary, [3]Parsons Laboratory, Massachusetts Institute of Technology, Cambridge, MA, USA, [4]HUN-REN Institute of Earth Physics and Space Science, Sopron, Hungary, [5]HUN-REN-ELTE Theoretical Physics Research Group, Budapest, Hungary, [6]Departamento de Ciências Atmosféricas, Instituto de Astronomia, Geofísica e Ciências Atmosféricas, Universidade de São Paulo, São Paulo, Brazil

Key Points:

- Schumann resonance (SR) frequency variations of the E_Z field component at nodal distances can be used to study global lightning dynamics at different time scales
- The movement of individual squall-line formations in South America can cause detectable variations in SR peak frequency at NCK, Hungary
- Extratropical extension of global lightning activity is revealed during the transition from warm to cold phases of the El Niño Southern Oscillation

Correspondence to:
T. Bozóki,
bozoki.tamas@hun-ren.epss.hu

Citation:
Sátori, G., Bozóki, T., Williams, E., Prácser, E., Mátyás, H., Albrecht, R. I., & Beltran, R. P. (2024). How do Schumann resonance frequency changes in the vertical electric field component reflect global lightning dynamics at different time scales? *Journal of Geophysical Research: Atmospheres*, *129*, e2024JD041455. https://doi.org/10.1029/2024JD041455

Received 25 APR 2024
Accepted 8 SEP 2024

Author Contributions:
Conceptualization: E. Williams
Data curation: H. Mátyás, R. I. Albrecht, R. P. Beltran
Resources: R. I. Albrecht, R. P. Beltran
Software: E. Prácser
Writing – review & editing: E. Williams

Abstract The electromagnetic waves in the Schumann resonance (SR) frequency range (<100 Hz) radiated by natural "lightning antennas" excite the Earth-ionosphere cavity confined between the Earth's surface and the lower ionosphere. The peak frequencies of SR are known to vary with source-observer distance (SOD), while the daily frequency range (DFR: $f_{max} - f_{min}$) is also indicative of the average size of thunderstorm regions. This paper provides observational evidence for these relationships based on SR frequency observations of the vertical electric (E_Z) field component at Nagycenk (NCK), Hungary in Central Europe from the period 1994–2015. Variations of the peak frequencies are considered on the annual, seasonal and diurnal time scales as well as during a specific event when squall-line formation of lightning activity in South America moves toward NCK. DFR is studied in relation to the El Niño Southern Oscillation (ENSO). Increasing area of lightning activity in mid-high Northern hemisphere latitudes has been identified by DFR variations during the transition from warm to cold episodes of the ENSO in 1998 and 2010. The extension of the lightning area is considered as a consequence of energy released in the tropics and exported to higher latitudes with some months of delay from the end of the El Niño episodes. The frequency variations are interpreted with model calculations and supported with satellite-based optical lightning observations (Optical Transient Detector, Geostationary Lightning Mapper). The described variations of SR peak frequencies and DFR yield information on the global/regional lightning dynamics and on this basis they have important application to climate issues as well.

Plain Language Summary Schumann resonances (SR) are global electromagnetic resonances maintained by global lightning activity in the cavity resonator formed by the Earth's surface and the lower ionosphere. This paper provides observational evidence for the relationships between the variations of SR peak frequencies of the first three resonance modes and the global/regional lightning dynamics on different time scales based on SR observations of the vertical electric (E_Z) field component. As lightning is one of the essential climate variables that provides valuable information on the state of the atmosphere, the lightning source-observer distance and lightning area-dependent frequency variations demonstrated in this paper have important applications to climate issues as well.

1. Introduction

The electromagnetic (EM) waves in the Schumann resonance (SR) frequency range (<100 Hz) radiated by natural "lightning antennas" excite the Earth-ionosphere cavity confined between the Earth's surface and the lower ionosphere (Schumann, 1952). In principle, continuous observation of SR spectral parameters (modal amplitudes/intensities, peak frequencies and quality factors) is suitable to monitor the worldwide lightning activity and the cavity properties even from a single station (e.g., Hobara et al., 2006; Kemp, 1971; Ogawa et al., 1968; Polk, 1969). The peak frequencies of the different SR modes and field components depend on the lightning source-observer geometry and the areal extension of lightning activity in the lossy Earth-ionosphere cavity, as well as on the cavity properties (Madden & Thompson, 1965; Nelson, 1967). The SR mode-specific amplitude/intensity structures attached to the active thunderstorm regions move with respect to the observer fixed on the Earth. The mode structures have nodal locations at specific distances from the active lightning source region,

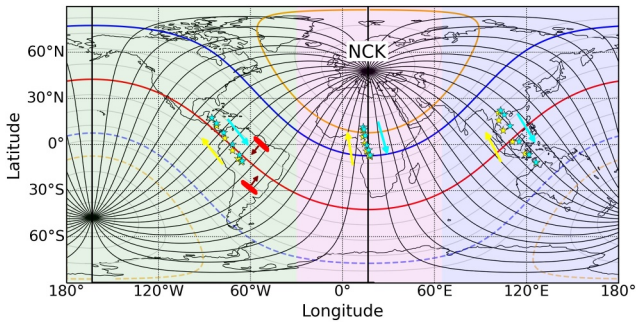

Figure 1. World map with three longitudinal ranges with greenish (America), reddish (Africa), and bluish (Asia) background containing the three tropical lightning chimneys. NCK is the location of the observer crossed with great circle paths (black) and circled with iso-distance curves (gray) with both sets of curves shown with 10° angular resolution. The red, blue, and orange curves mark the nodal distances of the vertical electric field component from NCK. The turquoise and yellow symbols indicate the hypothetical centers of the lightning distributions for each month of a year. The turquoise and yellow arrows are oriented to the direction of seasonal migration. The red symbols in South America represent squall-line type lightning distributions with red arrows showing the direction of their motion.

where the amplitude/intensity values are diminished and the frequencies become highly variable with increased/decreased values near the characteristic mode-specific eigenfrequencies (~8 Hz, ~14 Hz, ~20 Hz, …). In this paper, we make use of these substantial frequency variations associated with thunderstorm motion with respect to the nodal lines to study global lightning dynamics. The daily frequency range (DFR: $f_{max} - f_{min}$) is related to the size of the area where lightning discharges occur. The larger the area, the smaller the DFR becomes, and vice versa (Nickolaenko & Rabinowicz, 1995).

The peak frequencies observed in measured SR frequency spectra are distinct from the eigenfrequencies of the lossy Earth-ionosphere cavity as the propagating waves, which excite the cavity, are always present simultaneously with the standing waves (eigenmodes) (Kulak et al., 2006; Sentman, 1996). The mode structures of the EM field components are basically determined by the standing waves which have nodal lines in mode-specific angular distances from the excitation source. The location of the nodal lines in the lossy Earth-ionosphere cavity become observable due to the propagating waves with non-zero field amplitudes and highly changing frequencies in these regions. Theoretically the source-observer distance (SOD) dependence of the SR frequencies is described by the complex Legendre-function or as a series of real Legendre polynomials (Bliokh et al., 1980; Kulak et al., 2006; Nickolaenko & Hayakawa, 2002; Prácser et al., 2019; Sentman, 1996; Wait, 1996). The SOD-dependent frequency variations of SR were already discussed by multiple authors (Balser & Wagner, 1960; Galejs, 1970, 1972; Jones, 1969; Madden & Thompson, 1965; Nelson, 1967). The theoretical distance-dependent frequency variation of the first E_Z mode in a uniform lossy cavity was presented using single circular sources with different diameters (Nickolaenko & Hayakawa, 2002, Figure 4.20).

It is important to emphasize that while there is no nodal line associated with the first magnetic mode (the frequency increases monotonically with SOD), in the case of the E_Z field component the first mode already has a nodal line at 90° from the source. A number of studies have exploited the former property of the magnetic field to estimate the north-south migration of global lightning activity on the annual timescale, based on observations of the frequency of the first magnetic mode (e.g., Koloskov et al., 2020, 2022; Nickolaenko et al., 2015). The present study, on the other hand, links the substantial frequency variations around the nodal lines to changes in the spatial distribution of global lightning activity and the associated SOD changes. Therefore, for our approach, it is advantageous to use electric measurements, and it is also important that the NCK station is often located in a nodal position for the different modes with respect to global lightning activity (see Figure 1).

Observational evidence for the SOD-dependence of SR peak frequencies is limited in the literature. Nelson (1967) attributed an unusual peak frequency variation of the E_z field component recorded in the USA (Westford, Massachusetts) to the proximity of a nodal line to the SR site with respect to African lightning sources. The first utilization of the peak frequency variation at a nodal distance in exploring global lightning dynamics was given on the ENSO time scale (Sátori & Zieger, 1999). The southward shift of global lightning was indicated by the frequency variation of the third E_Z mode at Nagycenk (NCK), Hungary in Central Europe at the nodal distance from the African lightning chimney during the super El Niño event of 1997/98. Independent Optical Transient Detector (OTD) satellite observation for two cold (1996, 1999) and two warm (1997/1998 and 2002/2003) ENSO episodes supported the meridional displacement of global lightning (Sátori, Williams, & Lemperger, 2009).

Sátori and Zieger (2003) showed that the diurnal frequency patterns of the E_Z field component are characteristic for a season and the length of the time interval with repeated frequency patterns corresponds to the length of the "electromagnetic seasons." Nickolaenko (2015a) demonstrated the diurnal-seasonal reproducibility of SR parameters from year to year based on the observation of the E_Z field component at NCK. Nickolaenko (2015b) presented an alternative interpretation (source migration or ionospheric height variation) for the changes of SR spectral parameters at the Ukrainian Antarctic station "Akademik Vernadsky." Nickolaenko et al. (2015) analyzed long-term magnetic records (2002–2011) from the same polar station. They found that the annual changes of SR frequencies and intensity are the manifestation of a north-south migration of global lightning activity. They also discussed the inter-annual variations of SR frequency and intensity both attributed to the solar

activity, and confirmed the multi-station frequency response to the solar cycle described by Sátori et al. (2005). Koloskov et al. (2020) studied the seasonal and inter-annual variations of SR signals simultaneously observed from an Antarctic and an Arctic station. They showed that "the seasonal changes in peak frequencies are determined by the regular meridional drift of the world's thunderstorm centers up to ±(18°–26°) in latitude from the equator." They found that global thunderstorms are independent of the solar cycle phase. The observed inter-annual variations originate from changes in the lower ionosphere driven by the 11-year cycle in the solar activity. Koloskov et al. (2022) stated the unequal duration of the "electromagnetic seasons" based on the Arctic/Antarctic observations of the magnetic field components which confirmed the result of Sátori and Zieger (2003).

DFR values can be determined from frequency variations of the E_Z field component indicating areal changes in global lightning on the diurnal time scale. It follows that the highest time resolution of the DFR parameter is one day. Areal variations of global lightning were discussed on the annual and seasonal time scales based on DFR changes of E_Z records at NCK in 1994–1995 by Nickolaenko et al. (1998). Areal variations of global lightning were also deduced from DFR records at NCK for longer time scales: for 1994–2002 by Sátori and Zieger (2003) and for 1994–2012 by Sátori et al. (2013).

In this paper we show that in the lossy Earth-ionosphere cavity of the real world, the value of the actual modal peak frequency is strongly affected by that active thunderstorm region which is in the vicinity of the mode-specific nodal distance from the observer and moves toward or away from the observer. The frequencies exhibit relatively high or low values, departing by some tenths of Hz from the mean frequencies in that time interval when the observer lies in a nodal position with respect to the active lightning source region. Observational evidence is provided for the relationships between the variations of SR peak frequencies and distance changes of active thunderstorm regions (tropical chimneys) on the annual, seasonal and diurnal time scales as well as during a specific event when squall-line formation of lightning activity in South America moves with respect to the SR observer at NCK located in the nodal region of the squall-line. DFR is studied on the ENSO time scale. All these frequency variations yield information on the global/regional lightning dynamics and on this basis they have important application to climate issues as well.

The paper is structured as follows. The SR data and satellite-based lightning information are introduced in Section 2. Section 3 describes the location of the NCK observer and its nodal distances with respect to the distribution of global lightning activity, while Section 4 presents the model calculations used to understand the SR frequency variations introduced by global lightning dynamics. Section 5 and 6 contain our observational results on the annual/seasonal and diurnal time scales, while Section 6 presents a case study of the effect of an individual squall-line in South America on SR frequencies observed at NCK. Section 7 is devoted to the DFR variations during the sharp transition from warm to cold ENSO episodes in two cases (in 1998 and 2011) between 1994 and 2015. The final two sections of the paper (Section 8 and 9) discuss and summarize our results.

2. Data and Methods

2.1. SR Data

SR frequencies and amplitudes of the first three modes (~8 Hz, ~14 Hz, ~20 Hz) of the E_Z field component have been recorded at the Széchenyi István Geophysical Observatory, also known as the Nagycenk Geophysical Observatory (NCK; 47.6°N, 16.7°E) in Hungary, Central Europe since May 1993 using a very stable ball antenna, a preamplifier with high input impedance and a low noise amplifier, and a personal computer with multi-channel A-to-D-converter (Sátori et al., 1996). The spectral method used at NCK works in the time domain and is based on a filtering technique known as complex demodulation (Banks, 1975; Beamish et al., 1979). The phase and amplitude of the complex wave vector are determined in time intervals corresponding to the central period of pre-selected frequency ranges: 7–9 Hz, 13–15 Hz and 19–21 Hz. The sampling rate is 100 Hz. Using this spectral technique, the SR peak frequencies and amplitudes are determined in the frequency range of the first three SR modes (Sátori et al., 1996). The method was tested with observations (Sátori, 1996; Sátori et al., 1996). Under locally undisturbed conditions, 52 (60 from the year of 2020) time windows of 35.8 s each are evaluated in one hour while altering the sampling and filtering processes. The number of filtered complex wave vectors is 298, 512, and 716 for the first, second, and third modes, respectively, in a time window in an optimum case (all amplitudes are accepted) which assures the high accuracy of the estimated frequency values. The standard deviations of the hourly frequency averages are ±0.008–0.012 Hz for the first mode, ±0.010–0.018 Hz for the

second mode and ±0.016–0.030 Hz for the third mode under locally undisturbed conditions in the vicinity of the SR ball antenna at NCK.

2.2. OTD/LIS Lightning Data

The OTD was launched in 1995 aboard the MicroLab-1 satellite into a near polar orbit at an inclination of 70°, and operated until 2000. It detected both intra-cloud and cloud-to-ground discharges during day and night conditions with a high detection efficiency. The instrument was very suitable for studying global lightning patterns and how they changed with time (Christian et al., 2003). It surveyed virtually all areas of the globe where lightning normally occurred. In the recent study, the meridional distribution of global lightning observed by the OTD is utilized to support the DFR variations at NCK in some specific months of the Super El Niño event of 1997/1998 as compared to the same months of the adjacent years. OTD observations are also used to infer the hypothetical centers of global lightning activity for each month of the year in order to support the interpretation of SR frequency variations on the annual/seasonal time scale.

The Lightning Imaging Sensor (LIS) onboard the NASA TRMM satellite was also a space-based instrument used to detect the distribution and variability of total lightning (cloud-to-cloud, intra-cloud, and cloud-to-ground lightning), but the monitored area was confined to the tropical/subtropical belt between ∼30°N and ∼30°S latitudes which, however, includes the three most important tropical lightning regions. In this paper, the OTD records for the years of 1995–2000 and combined OTD/LIS observations of total lightning for the period 1998–2004 in 2.5° × 2.5° grids are used to support the understanding of the mean SR frequency variations on the diurnal time scale in January.

2.3. GLM Lightning Data

The Geostationary Lightning Mapper (GLM) is a single-channel, near-infrared OTD that has been in operation since March 2017. GLM measures total lightning activity continuously over the Americas and adjacent ocean regions with near-uniform spatial resolution of approximately 10 km (Goodman et al., 2013). The GLM identified a squall-line formation of lightning in South America on 15 February 2023 which is studied by SR frequency observation at NCK in this paper.

2.4. WWLLN Lightning Data

The World Wide Lightning Location Network (http://wwlln.net) is a collaboration among over 50 universities and institutions for providing lightning locations based on a global network of very low frequency radio receivers. In this paper, Word Wide Lightning Location Network (WWLLN) data are used to confirm the extratropical extension of global lightning activity in the warm-to-cold transition following the warm El Niño period of 2010.

2.5. ENS-ONI Index and Surface Temperature Data

DFR variations are analyzed on the ENSO time scale in this study, using the Ensemble Oceanic NINO Index (ENS-ONI) index to characterize the ENSO phenomenon (https://www.webberweather.com/ensemble-oceanic-nino-index.html). The global context of the tropical ENS-ONI index is demonstrated by presenting the record of global monthly mean surface temperature change from NASA (https://data.giss.nasa.gov/gistemp/graphs_v4/) on the same time scale.

We also utilize the HadCRUT5 data set (Morice et al., 2021) to investigate changes in the meridional distribution of surface temperature on the ENSO timescale. This data set provides broader coverage in regions with sparse data and enhancements in observed areas as compared to HadCRUT4. It combines near-surface air temperature measurements from land-based weather stations with sea surface temperature measurements from ships and buoys. These measurements are transformed into surface temperature anomalies relative to the 1961–1990 reference period, covering the entire globe. To determine absolute temperatures, we rely on the CRU climatology (Jones et al., 1999). We used the Climate Data Operator to calculate the meridional temperature distributions.

3. The Location of E_Z Nodal Distances in Case of the NCK Station

Figure 1 shows the position of the NCK observer on the globe with iso-distance curves around the site and great circle paths perpendicular to them. The location of nodal lines can be estimated by using Legendre polynomials, $P_{n = 1,2,3\ldots}(\cos\theta)$ (Erdelyi, 1953), where θ is the angular distance between the source and observer along the great circle path. Their zero values indicate the nodal distances of the resonance modes. The red curve on Figure 1 refers to the 90° nodal distance of the first E_Z mode where $P_1 = \cos\theta = 0$, the blue one indicates the nodal distance of 54.73° where $P_2 = 0.5*(3*\cos\theta^2 - 1) = 0$, and the orange curve shows the nodal distance of 39.23° where $P_3 = 0.5*(5*\cos\theta^3 - 3*\cos\theta) = 0$ around NCK. The NCK station is located in the nodal position if lightning sources become active in such angular distances. The third mode has a common (second) nodal distance with the first mode at 90°. The dashed blue curve indicates the second nodal distance of the second mode at 125.27°, and the dashed yellow curve corresponds to the third nodal distance of the third mode at 140.77° from NCK. These two nodal lines mostly avoid the lightning active areas of the Earth. Note that an electric antenna is responsive to lightning sources in any direction from the observer in contrast to magnetic measurements which are only sensitive to lightning sources in specific directions. The turquoise and yellow symbols indicate the hypothetical centers of the lightning distribution for each month of a year in the longitudinal range of the three main tropical lightning regions. The three longitudinal ranges were defined as 65°–180°E for Asia/Maritime Continent (AS/MC), 30°W–65°E for Africa (AF) and 180°W–30°W for the Americas (AM), and correspond to the selection of longitudinal ranges given in the paper of Christian et al. (2003). The location of hypothetical centers for each month was determined from OTD satellite observations by calculating the center (weighted average) of the lightning distribution in the given longitudinal ranges over the entire 90°S–90°N latitude range for the years 1995–2000. We note that a number of studies has shown that total lightning distributions provided by the OTD/LIS satellites are largely consistent with SR observations (e.g., Boldi et al., 2017; Füllekrug, 2021; Sátori, Mushtak, & Williams, 2009).

The yellow arrows indicate the direction of motion of the lightning centroids from the Southern Hemisphere (SH) to the Northern Hemisphere (NH) and the turquoise arrows show the opposite direction of lightning migration during the year. The red symbols with arrows in South America represent squall-line type lightning distributions moving perpendicularly to the 90° nodal line away/toward the NCK observer. It can also be seen that the Asia/MC lightning sources also move perpendicularly to the 90° nodal line and cross it twice a year during the seasonal migration. The African lightning never reaches the 90° nodal distance but it approaches or crosses the 55° nodal distance of the second mode and crosses the third mode's 40° nodal line twice in a year. The lightning sources of the Americas migrate more or less parallel to the 90° iso-distance curve during the whole year and consequently their distances are rather stable with respect to the NCK observer. The motion and migration of lightning sources with different directions outlined here are accompanied by variations of SR peak frequencies of the first three electric modes observed at NCK which are attributed to the distance changes between the lightning source and the NCK observer. In the next section, we present model calculations to understand and interpret the observed frequency variations at NCK.

4. Model Calculations

We need to present the theoretical background of the SOD dependence of SR frequencies to understand and interpret the observed variations of modal peak frequencies (f_1, f_2, f_3) at NCK on the different time scales. For this purpose, we use our open-source python package called "schupy," which enables calculating theoretical SR spectra for arbitrary source-observer configurations (Bozóki et al., 2019). The model applies the solution of the 2-D telegraph equation for the uniform Earth-ionosphere cavity (see e.g., Prácser et al., 2019) characterized by two complex, frequency-dependent altitudes (He/Hm representing the electric and magnetic altitudes, respectively, see Mushtak & Williams, 2002 for more details), and is capable of modeling extended sources represented by randomly distributed point sources within the given radius from the center of the source (100 point sources are distributed in this case, forming a uniform distribution of points on the sphere within the given radii). For the present study, simulations were performed with source radii of 1.5, 1.8, 2.0, 3.0, and 4.0 Mm, and theoretical SR spectra were calculated with a frequency resolution of 0.1 Hz between 1 and 48 Hz. In terms of the SOD, we covered the range from 20 to 140° with a resolution of 0.5°. In order to extract modal peak frequencies corresponding to the first three SR modes, after applying a quadratic interpolation on the spectra to increase the frequency resolution to 0.01 Hz we looked for spectral peaks in the following bands: f_1:6–10 Hz, f_2:11–16 Hz, f_3:18–22 Hz. Figure 2 shows our simulation results with different

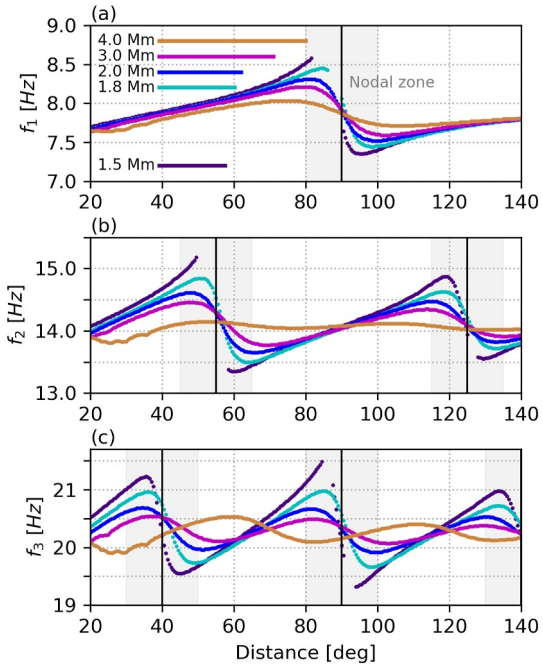

Figure 2. Source-observer distance dependent frequency variations of the E_Z field component for the (a) first, (b) second, and (c) third Schumann resonance mode computed for circular source regions (including 100 randomly distributed point sources) with different radii given in Mm. The light gray strips indicate the nodal zones in which the frequencies depart most strongly from their mean values. In the nodal zones, some missing frequency values can be noted (especially for the narrower sources), which could not be determined due to missing local intensity maxima in the analyzed frequency bands.

source radii for the first three SR modes. The light gray strips of 20° angular degree widths indicate the nodal zones around the mode-specific nodal lines of the E_Z field component. The nodal zones cannot exactly be defined because their width is different for the different source sizes and it also depends on the mode number. It can be seen on Figure 2 that the larger is the source area the narrower is the frequency range in the nodal zones, and vice versa. In the limit of very large source size, the frequency range is expected to vanish.

5. Annual/Seasonal Frequency Variations of the E_Z Field Component

5.1. First E_Z Mode

Figure 3a shows the monthly mean frequency values (single value in each month) of the first E_Z mode at NCK during two solar cycles in the interval 1994–2015. A clear frequency response of ionospheric origin for the 11-year solar cycle can be observed in the record with minimum values at solar minimum (1996, 2009/2010) and maximum values at solar maximum (2002). This effect was already discussed mainly by Sátori et al. (2005). On the annual timescale the monthly means of the f_1 frequency exhibit maxima in NH summer and minima in NH winter from year to year (Figure 3a), only the mean frequency levels of the annual frequency variations are shifting upward/downward at solar maximum/minimum ($\lesssim$0.06 Hz, see Figure 3a). To understand this annual frequency response, we computed the monthly mean frequency values for the maximum activity of each tropical lightning chimney (AS/MC: 07–10 UT, AF: 14–17 UT, AM: 20–23 UT) because they have different distance-relations with respect to the nodal distances indicated in Figure 1.

It can be seen that only the frequencies observed at the maximum activity of the Asia/MC tropical chimney between 07 and 10 UT exhibit a pronounced annual variation with NH summer maximum and NH winter minimum (Figure 3b), and with relatively large frequency differences (~0.15 Hz) between the two seasons. In contrast, the frequencies at the maximum activity of Africa (14–17 UT) show noisy and rather opposite behavior (minimum at NH summer and maximum at NH winter in some years) with small frequency differences (~0.05 Hz) between the two seasons (Figure 3c). The African lightning activity has the shortest distance variation between NH summer and winter (see Figure 1), so the noisy frequency is likely due to the random-like changes in the position of the active lightning areas with respect to NCK and the small variation of FL of ionospheric origin ($\lesssim$0.06 Hz) (Sátori et al., 2005). Apart from the solar cycle variation the frequencies in the hours of the maximum activity of the Americas indicate only some fluctuation without characteristic and robust annual variations (Figure 3d). This frequency variability is attributed to the source proximity of the 90° nodal distance from NCK in the whole year.

Now we can interpret the annual frequency variations of the first E_Z mode collected in annual time windows for the time period of the maximum activity of each thunderstorm region (Figures 4a–4c). For this purpose, we cut annual time windows (from January to December) in consecutive years from the long-term records displayed in Figure 3 and superimpose them to see the general behavior of frequencies on the annual time scale. We did not remove the frequency variations of ionospheric origin, therefore the variation of frequency levels (thin curves) running above and below their mean values contain the solar cycle variation. These latter variations do not influence the magnitude, shape and sign of the mean frequency change on the annual time scale. We compare the measured values with the model calculation shown in Figure 4d. As it has been described in Section 4, a single circular source was applied in the model calculations which correspond to a uniform Earth-ionosphere cavity with fixed ionospheric altitudes. Accordingly, only a qualitative comparison (relative frequency variations) is possible between the observed and modeled frequencies. The nearest (during NH summer) and farthest (during NH winter) distance values of centroids corresponding to the three topical lightning chimneys to NCK are marked with arrows in Figure 4d. The Asian/African lightning centroids migrate between the distances of 112° (AS-W)–72° (AS-S)/

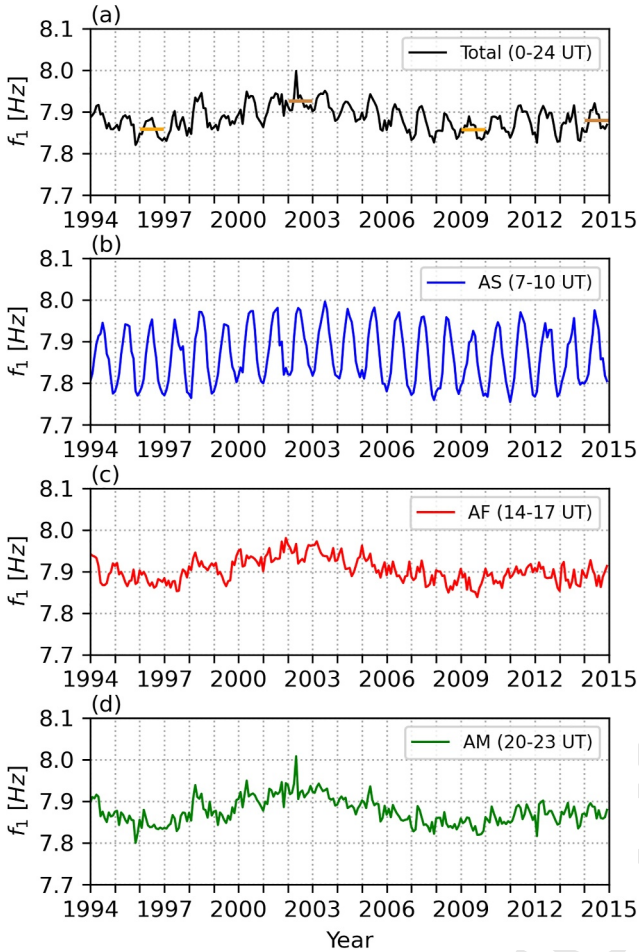

Figure 3. Long-term (1994–2015) frequency variations of the first E_Z mode at NCK, Hungary (a) for the whole diurnal cycle as well as for the time period of maximum lightning activity in panels (b) Asia/MC (07–10 UT), (c) Africa (14–17 UT), and (d) America (20–23 UT). In panel (a) horizontal lines indicate yearly mean frequency values in solar minimum (orange) and maximum (brown) years.

56° (AF-W)–36° (AF-S) on the seasonal timescale, while the American (AM) lightning centroid stays relatively fixed at around 90° (AM).

Considering the model calculation in Figure 4d, the hypothetical center of the AS/MC lightning chimney in NH winter (December/January) with lower frequency than in NH summer (June/July) is in accordance with the observations (Figure 4c). Both positions are close to the nodal zone with a center of 90° angular distance which is the nodal distance of the first E_Z mode at NCK. The frequency shows a considerable increase (~+0.6 Hz) with the closer position to NCK in NH summer as compared with the frequency computed for the NH winter position of the AS/MC chimney region. The model computation clearly shows the opposite behavior of frequency variation with smaller magnitude (~0.15 Hz decrease) for the African chimney region. The frequency is higher in NH winter and smaller in NH summer.

The annual variation of the monthly mean frequencies (Figure 3a) is the superposition of the frequency variation corresponding to the angular distances of the three chimneys from NCK. It is dominated by the highest frequency variation due to the nodal position of NCK with respect to the AS/MC chimney region. The modeled changes of frequencies were higher than the observed values because a single source with 3 Mm radius was only selected to compute the distance-dependent frequency variations. In the real world there are multiple sources which reduce the observed frequency range.

5.2. Second E_Z Mode

Figure 5 interprets the annual frequency variations in a similar way to Figure 4, but for the second E_Z mode. Africa is the only important tropical lightning source which is in quasi-nodal distance from NCK for the months November to March in the case of the second mode (see Figure 1). The nearest position of the hypothetical centroid of the African lightning chimney (~36°N) to NCK is in July. The second mode frequency decreases slightly when the April centroid is approaching the July centroid and the frequency increases slightly when the July centroid is shifting to the October position. Both the observations (Figure 5a) and the model calculation (Figure 5b) show these moderate frequency variations when the source is departing/approaching from/to the African fall/spring (AF-FS) season position. From November to March, NCK is in the nodal zone, indicated with a reddish area in the model computation (Figure 5b). The second mode frequencies become

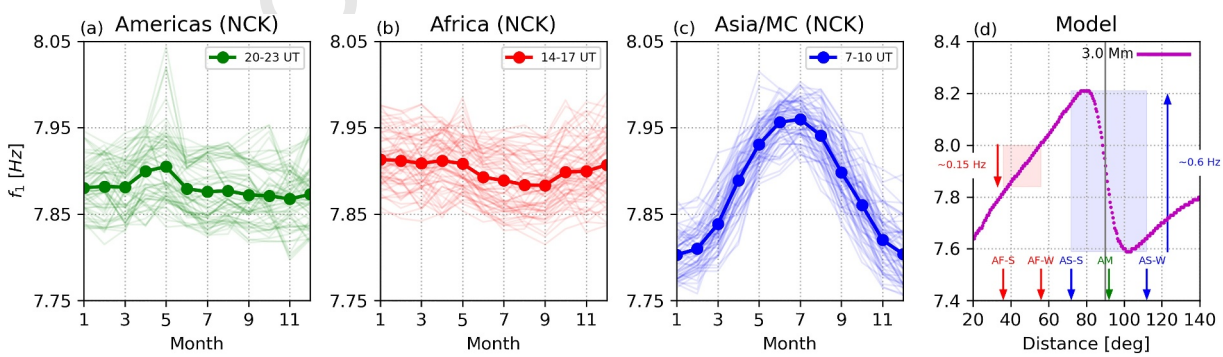

Figure 4. Frequency variations of the first E_Z mode on the annual time scale: (a) for the Americas (AM), (b) for Africa (AF), and (c) for Asia/MC (AS) at NCK in the hours of their maximum activity (from 1994 to 2010), and (d) modeled distance-dependent frequency variations between the Northern Hemisphere summer (S) and winter (W) source positions (AF-S and AF-W as well as AS-S and AS-W). The reddish and bluish background boxes in panel (d) represent frequency variations expected at the given source-observer distances in the African and Asian chimney regions in the different seasons.

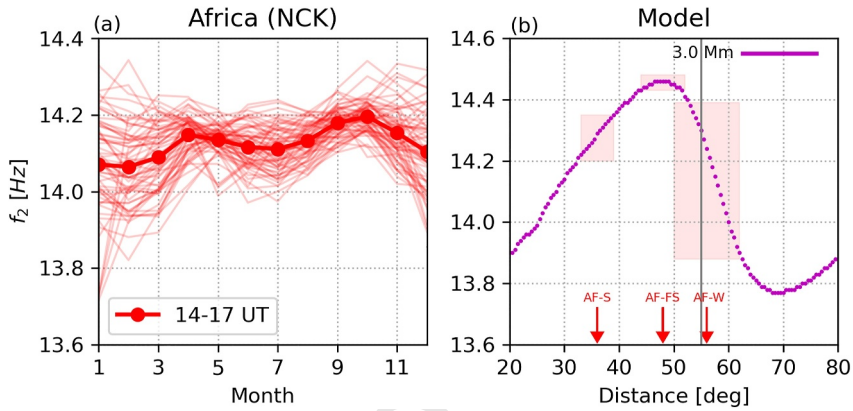

Figure 5. Frequency variations of the second E_Z mode on the annual time scale: (a) observations (from 1994 to 2010) and (b) modeled values. The reddish background boxes in panel (b) represent frequency variations expected at the given source-observer distances in the different seasons (NH-summer: AF-S; NH-fall/spring: AF-FS; NH-winter: AF-W).

highly variable in a rather wide frequency range which means that NCK has remained in the nodal zone for months (from November to March). It is noted that the small frequency variations of ionospheric origin are also included in the frequency changes in those months (thin lines).

5.3. Third E_Z Mode

Figure 6 shows the frequency variations of the third E_Z mode (~20 Hz) on the annual time scale. NCK is in nodal position twice in a year during the north-south seasonal migration in case of the African lightning source and in case of the Asia/MC source region, too, which has a common nodal distance at 90° (10 Mm) with the first E_Z mode. The model calculation (Figure 6c) show, in accordance with the observations, that the frequencies start decreasing from January (NH winter) in case of Africa and Asia/MC, they increase sharply up to their summer maxima in July (NH summer), and then return to the original FL in NH winter. NCK is in the nodal zone with respect to the third E_Z mode for almost the entire year and therefore the variability of frequencies is rather high in every month. An asymmetrical behavior of the frequency variations is noted between the spring and fall seasons for both chimney regions. The frequency variations show different temporal evolutions, with April frequency minimum for Africa and March frequency minimum in the case of Asia/MC. The fall frequency transitions also differ a little for the two lightning areas. These frequency variations indicate an asymmetrical migrational dynamics (source position) of lightning in these two transition seasons.

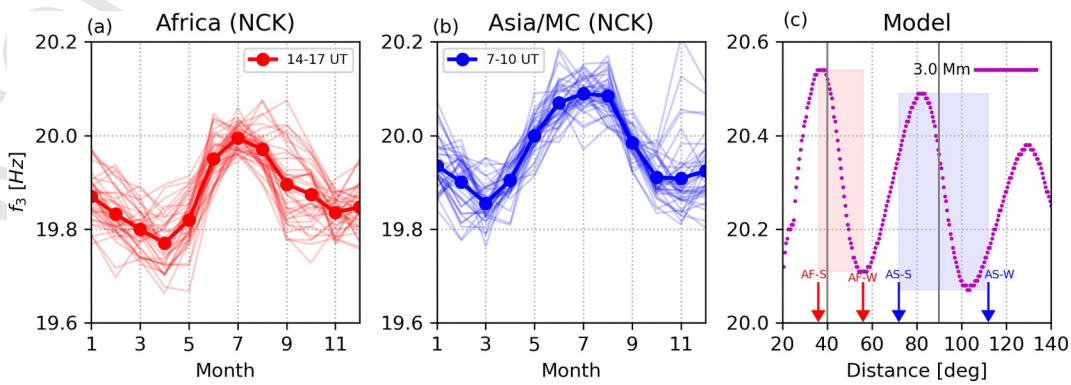

Figure 6. Frequency variations of the third E_Z mode on the annual time scale: (a) for Africa, (b) for Asia/MC (from 2000 to 2009), and (c) for the model computation. The reddish and bluish background boxes in panel (c) represent frequency variations expected at the given source-observer distances in the African and Asian thunderstorm regions in the different seasons. AF-S and AF-W as well as AS-S and AS-W indicate the Northern Hemisphere (NH) summer and NH winter positions of the African and Asian chimneys.

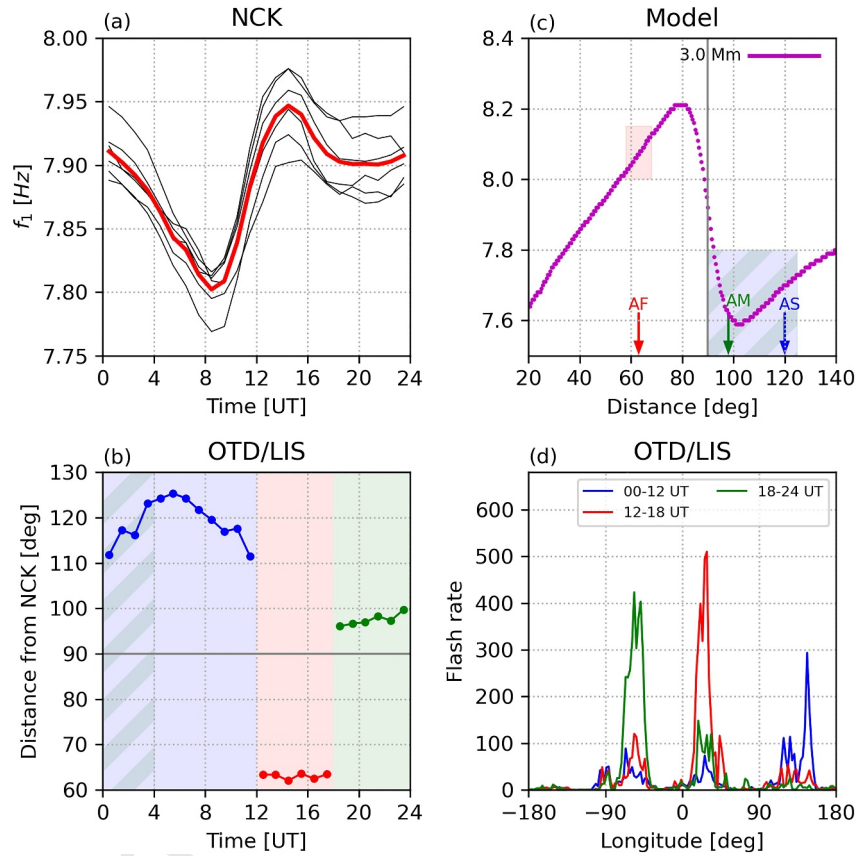

Figure 7. (a) Diurnal frequency variation of the first E_Z in January months (1995–2000). (b) Estimated source-observer distances of the three tropical chimney regions from NCK: bluish for Asia, reddish for Africa and greenish for America. The striped interval indicates a possible simultaneous activity of Asia and America. (c) Model calculation for the distance-dependent frequency variations indicating the position of the corresponding lightning region. (d) Average lightning activity (1998–2004) in three time intervals (00–12 UT, 12–18 UT, 18–24 UT) in a day with three different colors, each of them corresponding to the maximum activity of a tropical chimney. Note the simultaneous activity of the different chimneys in the displayed time intervals.

6. Diurnal Frequency Variations of the E_Z Field Component

The SR frequencies exhibit a large variety of diurnal shapes depending on the mode numbers and field components (Ondrášková et al., 2007; Sátori, 1996). In general, the shapes become increasingly complicated with higher mode numbers (Ondrášková et al., 2007; Sátori, 1996). Here we interpret the mean diurnal frequency variations of the first E_Z mode in January (NH winter) as it is the simplest one due to the rather confined chimney areas (source regions) in the SH in this month, with well-defined distances from NCK.

Figure 7a presents diurnal frequency variations for January for the years of 1995–2000. These curves can be characterized by deep frequency minima near 08–10 UT and by pronounced frequency maxima near 14–16 UT. Figure 7b shows the average angular distances of NCK from the hypothetical center of the three main tropical thunderstorm regions in January months (1998–2004) based on OTD/LIS observations. Figure 7b demonstrates which chimney activity is dominant in which time intervals of the day. Generally, each lightning chimney has maximum source intensity in the local afternoon (Blakeslee et al., 2014). However, it is noted that the lightning activity of a tropical chimney never switches on/off sharply. All lightning chimneys show more or less lightning activity simultaneously but with very different intensity during the different hours of a day as it is shown based on OTD/LIS observations in Figure 7d. The outermost lightning source relative to NCK is in Australia (Pacific Islands) and lightning activity slowly migrates in the northeast direction following the land areas of the Asia/MC chimney in early UT hours. The distance estimation of the source region is uncertain in the 00–04 UT time interval because the American chimney is still active and very close to the 90° nodal line while at the same time the

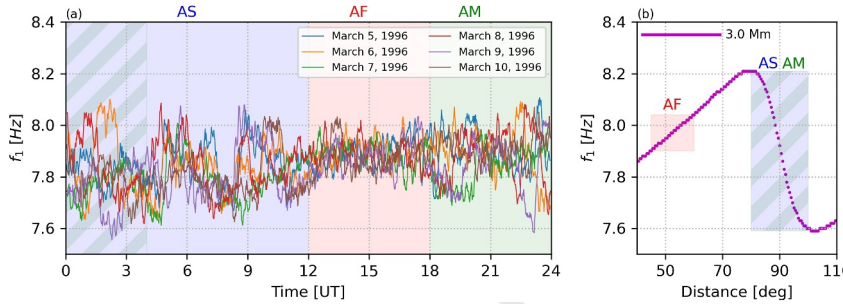

Figure 8. (a) Diurnal frequency variations of the first E_Z mode for six consecutive days in March 1996 smoothed with a five-point (~6 min) running mean. Colored backgrounds refer to the time intervals when the chimneys have their maximum lightning activity (bluish and greenish for Asia/MC and South America, reddish for Africa). (b) Model calculation of frequencies at nodal (Asia/MC and South America) and non-nodal (Africa) distances. The diagonal patterns indicate those hours in panel (a) and those angular distances in panel (b) when and where both Asia and America can simultaneously be active.

Pacific Islands and Australian lightning sources turn on at around 120° angular distance from NCK. A systematic decrease of distance (approaching to NCK) can be seen after 04 UT and up to ~11 UT when the Asian/MC lightning activity is first increasing and then diminishing. The model calculation presented in Figure 7c shows a systematic decrease of frequencies in a range of angular distances from 120° to 100° in accordance with the frequency observations between 00 and 10 UT (Figure 7a). The African lightning chimney begins to intensify at ~12 UT and it is very active in a quasi-stable angular distance of ~63° from NCK up to 17 UT. According to the model calculation a high frequency value belongs to this angular distance (Figure 7c), which is the highest one in the observations near 14 UT in January (Figure 7a). The South American chimney starts to be active from ~18 UT and it has the maximum intensity at ~21 UT and remains active up to early UT hours of the next day. The observed frequencies diminish after 18 UT but they do not decrease to the frequencies belonging to the ~100° angular distance of South America due to the higher frequencies of the remnant African lightning activity centroid at ~63° angular distance as shown in Figure 7d. In this time interval the NCK observer detects the average of the mixed frequencies corresponding to the two chimney regions (Africa and South America) at different angular distances from NCK.

It seems as if the global lightning makes a zonal migration around the globe as the maximum activity of each chimney occurs in local afternoon hours. However, this is only a virtual motion. Lightning activity of Asia/MC and America are increasing and diminishing in the lower frequency edge of the nodal region of the 90° nodal line while the African lightning activity is intensified and decreased on the higher frequency side of the nodal region of the 90° nodal line. But the lightning activity does not actually cross this nodal line (see Figure 7b), and that is why we call this a virtual motion.

Figure 8a presents diurnal frequency variations for six consecutive days in March when one may suppose that NCK is exactly in nodal distances from the Asian/MC and American lightning sources in case of the first E_Z mode, based on the location of their hypothetical centers shown in Figure 1. Highly variable frequencies appear in the early UT hours (00–11 UT) and in the late UT hours (18–24 UT) with random occurrence of different frequencies in these time intervals in the six consecutive March days. These are the two time intervals in a day when the Asian/MC and the American chimney regions have an increased (maximum) lightning activity. Some hundred-kilometer random-like changes in the position of activated lightning areas inside a chimney region cause unusually large frequency excursions (~0.6 Hz) over a short time interval (~1–2 hr) when the lightning sources are randomly crossing the nodal line. The African chimney is far from the first mode's nodal distance (90°, 10 Mm) (see Figure 1). Therefore the frequencies observed at NCK change in a rather stable frequency range (~0.2–0.3 Hz) between 12 and 18 UT when the African chimney is the dominant lightning source. All these frequency variations are supported by the model calculation shown in Figure 8b.

7. Frequency Variations Related to a Squall-Line in South America

A squall line is a linearly organized shape of thunderstorms. These elongated thunderstorm structures often contain frequent lightning, heavy precipitation, hail, strong straight-line winds, and occasionally tornadoes or

waterspouts. Giant squall lines in the South American tropics have long been recognized (Cohen et al., 1995; Garstang et al., 1994; Kousky, 1980). These systems tend to initiate on the sea breeze front at the edge of the Atlantic Ocean along the northeastern edge of the continent. The squall lines can propagate south-westward at speeds of 50–60 km/hr, sometimes as far as the Andes Mountains in less than two days, producing lightning continuously along the line for 1000 km or more. The "Pampero" is a regional wind that guides the motion of another squall-line type in South America which mostly affects Argentina and Uruguay and usually propagates from south-west to the north-east direction at speeds of 30–100 km/hr (Ludlam, 1980). Sometimes these storms also bring lightning and rain, and their passage is marked by a fall in temperature. The storms are steered by a south-westerly "pampero" wind, which follows a depression.

The location and geometry of the squall lines in South America have fortuitous connections with SR observations in Europe. First of all, the distance between the SR receiver (NCK) and the squall lines is often close to 10 Mm, which places the observer near the nodal region in case of the first and third E_Z modes for this range-confined source type in South America. Second, these lines tend to be oriented perpendicular to the great circle path linking the source and the observer. The SR frequencies can exhibit exceptionally large variations at the observer if the source is compact and at a nodal distance (see the model calculations in Figure 2).

Such exceptional SR frequency variations of the third E_Z mode was observed at NCK on 15 February 2023. Figure 9 shows the 30-min mean diurnal frequency and amplitude variations of the first three E_Z modes in the 10–20 February 2023 time interval (black line) as well as the corresponding standard deviation values (gray stripe). The red curves show the diurnal variations corresponding to 15 February 2023, with a noticeable frequency excursion in case of the third E_Z mode in early UT hours (00–09 UT) (Figure 9e). The frequency starts decreasing for some hours from 00 UT and then it is suddenly increasing for some hours (05–08 UT) before it returns to the mean FL. Considering the amplitude variations, it can be seen in Figures 9b and 9d, f that the amplitude values of February 15 (red curve) were lower than the mean values in most of the hours with the exception of the second mode which almost coincided with the mean curve. The largest amplitude decreases appeared in the case of the first and third E_Z mode around the 06–09 UT time interval (Figures 9b and 9f) when the largest frequency excursion occurred in the case of the third mode (Figure 9e). The mode-specific amplitude decrease is considered as the manifestation of the diminishing amplitudes at NCK which is in the nodal region with respect to a squall-line in South America. We note here that the first and third modes have common nodal distance at 90° (see Figures 2a and 2c). The first mode frequency does not show observable extraordinary excursion in the 06–09 UT time interval probably due to the less steep gradient of frequency variation than for the third mode in the same SOD range (see the model calculation in Figure 2 for 1.8 Mm source radius around 96°–100° angular distance for the first and third mode).

The GLM instrument observed a well-developed squall-line formation moving slowly from the southwest to northeast in the same hours documented in the white squared windows (Figure 10a) and in their enlarged forms from hour to hour (Figure 10b) in 00–09 UT hr when the anomalous frequency variations were observed at NCK in >10 Mm distance from that squall-line. The white stars indicate the positions of the lightning centroids. The squall-line spanned about 1200 km and the width was about 40–60 km according to the GLM observation. The latter dimension has a key role from the point of view of the observed frequency variation because this narrow part of the source determines the magnitude of the frequency variations when the squall-line is moving toward the NCK observer within the nodal region. However the single-source uniform model used in this study can't produce frequency values in the nodal region for source-sizes with <1.5 Mm diameter for lack of spectral power at these source-observer distances (see Figure 2). Figure 10c shows the modeled frequency variations of the third mode for two source-dimensions (1.8 and 2 Mm) in the nodal region and the rectangular window placed on the turquoise curve marks the location of the squall-line in the interval 00–09 UT on 15 February 2023. This figure again clearly demonstrates that the expected changes in SR frequencies are significantly larger for narrower sources.

The enlarged time window in Figure 10d enables a closer inspection of the frequency variation during the migration of the squall line from its farthest position (~101°) to the nearest location (~98°) with respect to NCK given in angular distances. The frequency began to decrease from 00 UT until ~04 UT, then to increase sharply until ~07 UT, and finally returned to the mean FL at ~09 UT as shown in Figure 10d. The observed frequency variation was about 0.4 Hz in those hours while the modeled frequency change was only 0.1 Hz due to the source-size problem in the single-source, uniform model described above. It is noted that the squall-line lightning remained at 09 UT but the strong intensification of lightning activity in the Asia/MC chimney after 07 UT

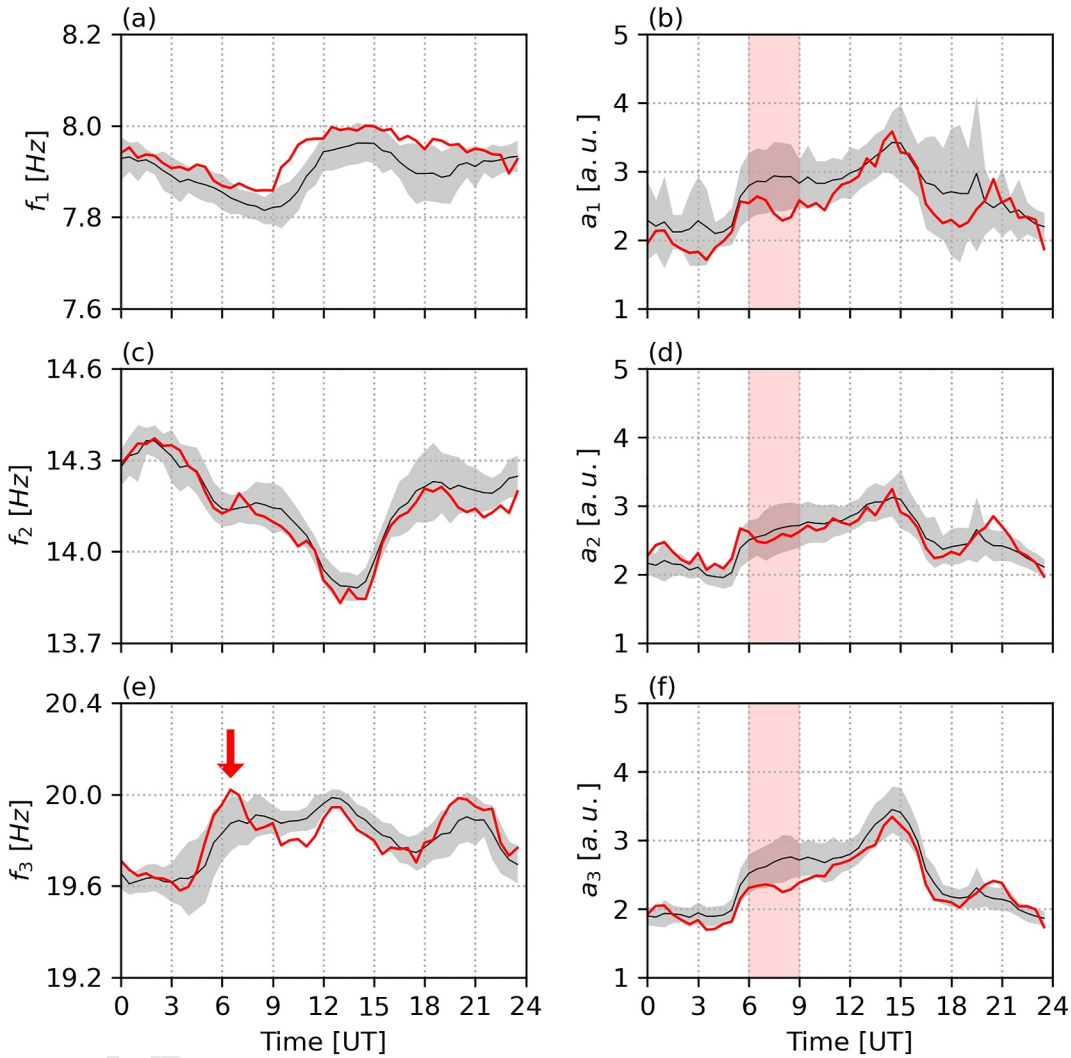

Figure 9. Mean diurnal frequency and amplitude variations of the (a)–(b) first, (c)–(d) second, and (e)–(f) third Schumann resonance modes of the E_Z field component at NCK in the 10–20 February 2023 time interval (black line) as well as the corresponding standard deviation values (gray stripe). The red curves show the diurnal variations corresponding to 15 February 2023. The red arrow in panel (e) shows an anomalous increase in the third E_Z frequency on 15 February in the 6–9 UT time interval, while the light red windows in panels (b), (d), (f) highlight amplitude values in the same time interval.

probably smoothed the frequency variation attributed to the squall-line source in South America on 15 February 2013. The SOD variation versus time (Figure 10e) enabled the calculation of the speed of the squall-line toward NCK. The estimated average speed was 35–40 km/hr in the time interval 00–09 UT.

8. Variations of the Daily Frequency Range During the Transition From Warm to Cold ENSO Episodes

Changes of lightning activity on the ENSO time scale were studied in numerous papers both in regional and global context (e.g., Ahmad & Ghosh, 2017; Chronis et al., 2008; Clark & Cecil, 2024; Goodman et al., 2000; Hamid et al., 2001; Kulkarni & Siingh, 2014; Kulkarni et al., 2015; Kumar & Kamra, 2012; Sahu et al., 2022; Sátori, Williams, & Lemperger, 2009; Sátori & Zieger, 1999; Tinmaker et al., 2017; Williams, 1992). These papers mainly focused on complete cold and/or warm ENSO periods. Recently, Williams et al. (2021) revealed the importance of the transition from cold to warm ENSO episodes in the case of two Super El Niño events (1997/1998 and 2015/2016) showing highly increased lightning activity in those periods. Here we study the areal variations of global lightning in the transition from warm to cold ENSO episodes for two cases based on DFR

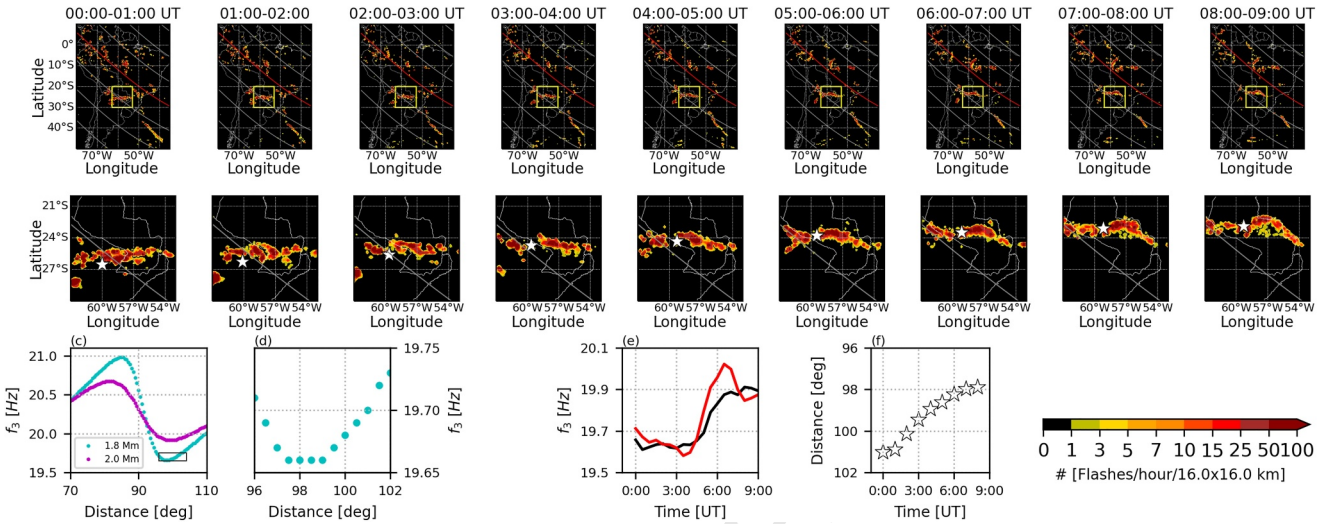

Figure 10. (a) Lightning activity within a selected area in South America in the first nine UT hours on 15 February 2023 as observed by the Geostationary Lightning Mapper (GLM) instrument. (b) Same as in panel (a) but for a smaller area (white boxes in panel (a)). (c) The modeled frequency variation versus source-observer distance (SOD). (d) Same as in panel (c) but within a shorter distance range in the model. (e) Observed frequency variations of the third E_Z mode in the interval 00–09 UT on 15 February 2023 (red curve) and the 10–20 February mean curve (black). (f) SOD variations versus time referring to NCK as inferred from the GLM observations.

variations. One of them is the end of the 1997/1998 super El Niño in May 1998, while the other is the termination of the second strongest El Niño in the studied years between 1994 and 2015 in April 2010 (Figure 11a). The sudden termination of the warm phase is characteristic for both selected cases. The global monthly mean surface temperature record shown in Figure 11b demonstrates a well-known result that El Niño events transfer heat from the ocean to the atmosphere (Trenberth et al., 2002), a process that ultimately warms the global atmosphere. Accordingly, the peak El Niño times in Figure 11a tend to lead the maxima in global air temperature by a few months.

Figures 12a and 12b show the ENS-ONI index in the two selected time windows (1996–2000 and 2008–2012). The colored background strips mark those months in which the mean DFRs are considered and intercompared. The cyan strips are assigned to June–July 1998 and May–June 2010 indicating those two months when the cold

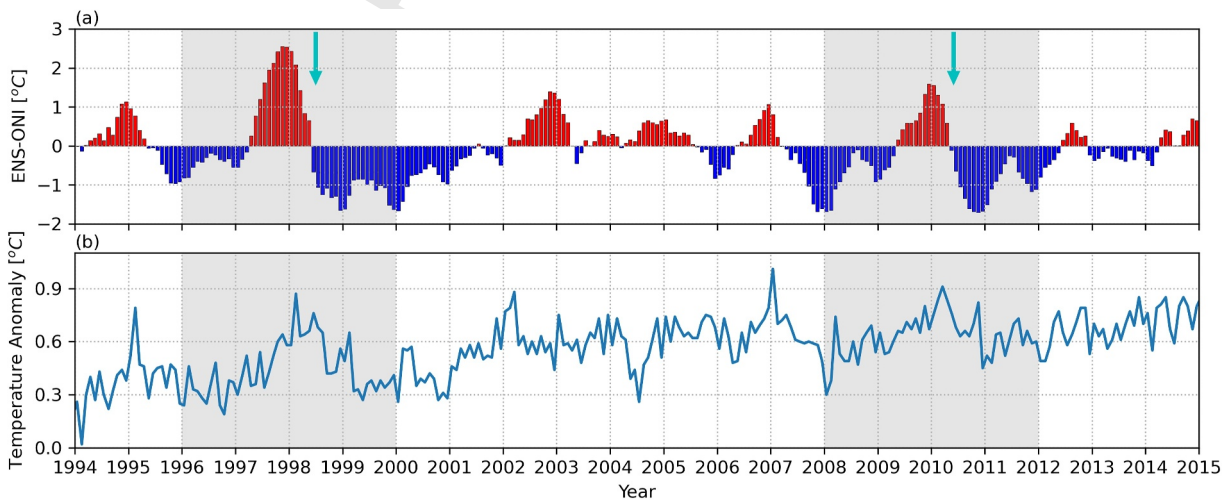

Figure 11. (a) The Ensemble Oceanic NINO Index (ENS-ONI) (red color indicates the warm phases while the blue color shows the cold phases) and (b) the global monthly mean surface temperature change in the time period of 1994–2015. The light gray background strips mark the two time windows (1996–2000 and 2008–2012) selected for a closer inspection of daily frequency range variations during the warm to cold transitions (cyan arrows) and for comparisons with the other phases of the El Niño Southern Oscillation events in the same time periods.

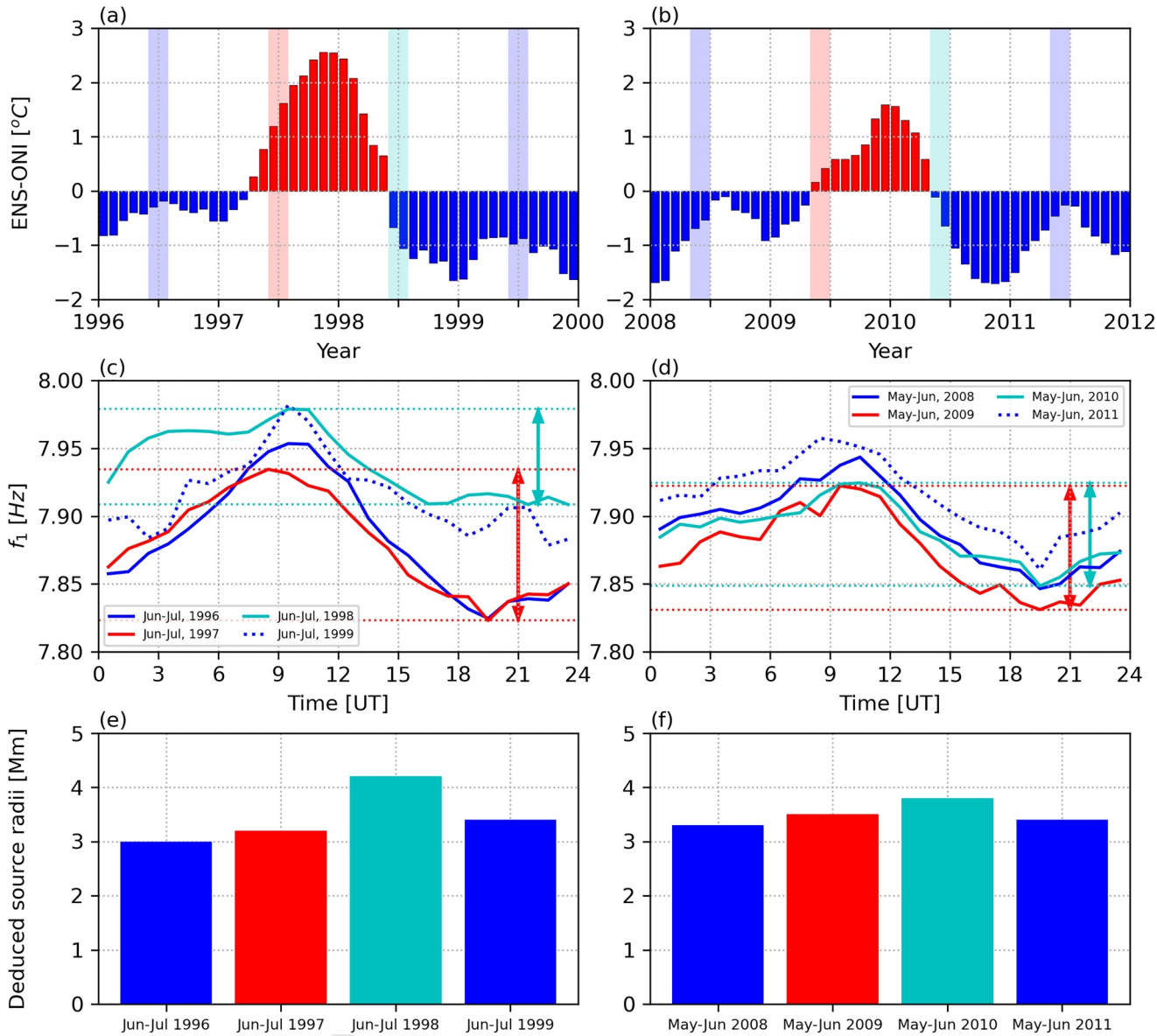

Figure 12. (a) and (b) present the ENS-ONI index in the two selected time windows (1996–2000 and 2008–2012). The colored background strips mark those months in which the mean diurnal frequency variations are considered. (c) and (d) exhibit the mean diurnal frequency variations of the first E_Z mode at NCK under different El Niño Southern Oscillation conditions in the two cases. Horizontal dashed lines indicate the maximum and minimum values of selected curves while the corresponding DFRs are indicated by double-headed arrows. (e) and (f) show the mean diurnal areal variations (deduced source radii) of the global lightning assigned to the daily frequency range changes in the selected 2-month time-intervals (see text for more details).

phase of ENSO episodes began following the sudden termination of the warm phase. The reddish background strips refer to the months under El Niño condition, and the bluish strips mark the months under La Niña condition. The June, July months in 1997, and the May, June months in 2009 fall rather at the beginning of the selected warm periods but we had to select the same months for comparisons to avoid aliasing by the annual/seasonal changes of DFR (Nickolaenko et al., 1998; Sátori & Zieger, 2003). Figure 12c and d show the mean diurnal frequency variations of the first E_Z mode at NCK under different ENSO conditions for the two cases. The DFR dependence on lightning area (i.e., the larger the area, the smaller the DFR becomes, and vice versa) is known from the literature (see the Introduction) and it is also demonstrated with model calculations using single-sources of circular shape with different source-radii in Figure 2. It can be seen on Figures 12c and 12d that the DFRs are the smallest immediately after the termination of the warm phase both in 1998 and 2010 in the selected months (turquoise arrows). The DFRs are larger in the beginning months of the warm period in 1997 and 2009 (red

arrows), and they are the largest in the months of cold episodes in 1996 and 1999 as well as in 2008 and 2011. The increased FL in Jun–Jul 1998 also indicates a northward shift of sources. This increased FL cannot be connected with the approaching solar maximum in 2000–2002 because the FL returned to a lower level in Jun–Jul 1999. In the case of the second event (Figure 12d), the SOD variation was not observed in 2010 and the highest FL in 2011 can rather be a manifestation of the starting approach to the solar maximum years of 2014/2015, as FL variations are indicative both for SOD variation and changes of cavity properties of ionospheric origin.

Nickolaenko and Rabinowicz (1995) developed an algorithm which produced calibration curves to convert DFR variations to areal changes (radii/diameter of a single source with circular shape). This algorithm was applied to determine the calibration curves for NCK to deduce the areal variations of lightning from DFRs on the annual/seasonal time scale by Nickolaenko et al. (1998). The same calibration curve for the first E_z mode was used here to deduce the global areal variation on the ENSO time scale in the selected months for the two selected ENSO events, each with sharp termination of the warm episode. Figures 12e and 12f show the mean diurnal areal variations (deduced source radii) of the global lightning assigned to the DFR changes in the selected 2-month time-intervals. It can be seen that the radii of the deduced circle-shape lightning area increases at the beginning months of the warm ENSO episodes in 1997 and 2009 (red bars) and the maximum radii (area) appear at the beginning months of the cold phases in 1998 and 2010, just after the sudden termination of the warm periods. The time history of the areal lightning variation during the two ENSO events is rather similar but areal changes are more pronounced related to the super El Niño event of 1997/1998 than in the case of the 2009/2010 event, in accordance with their respective magnitudes.

Comparisons with independent global lightning observations were possible using OTD observations for the first case, while the WWLLN data were used for the second case. It is important to note that while OTD observed virtually all areas of the globe where lightning normally occurs with a steady detection efficiency around the years of the 1997/1998 super El Niño, WWLLN's detection efficiency around the years of the 2009/2010 El Niño has steadily improved as the network has been upgraded with new receiver stations (Hutchins et al., 2012). Therefore, while for the first case OTD data are presented for all four two-month time-intervals (June–July 1996, 1997, 1998, 1999) shown in Figure 12, for the second case the WWLLN data are presented only for the warm-to-cold transition (May–June 2010) and the preceding warm period (May–June 2009). The mean meridional distributions of global lightning during these periods are presented in Figures 13a and 13d.

For the 1997/98 super El Niño (Figure 13a), the meridional lightning distribution is rather similar in the two cold months in 1996 and 1999 (blue solid and dotted curves). The maximum lightning activity appears in the June–July months of 1997 but it confines to the tropical belt in some degrees of NH latitudes and around 30° SH latitudes (red curve). These maxima decrease to the level of lightning activity in the cold periods however a highly increased lightning activity was observed at mid-high NH latitudes between 30° and 70° after the sudden transition between the warm and cold phases in June–July months of 1998. This significant increase and northern migration of lightning activity is linked, for example, to Siberia, where the number of lightning strokes has increased dramatically during this period (based on OTD maps not shown here). This process is also clearly demonstrated in Table 1, which shows the centroid latitude positions of global lightning activity for the months shown in Figure 13a. The centroid weights (total flash rates) are also listed in Table 1 with maximum total lightning in June–July of 1998, but the SR intensity values at NCK did not resolve this ∼10% increase of lightning activity probably due to nearby (European) thunderstorms around NCK. In the second case (Figure 13d), the increase of lightning activity is also observed at mid-latitudes, around 20 and 40 N latitudes.

The OTD and WWLLN observations support the known result that the thermal energy released during the warm ENSO periods has some months delay and extends to extratropical regions (Trenberth et al., 2002) to contribute appreciably to global warming. This interpretation is also supported by the meridional distribution of surface temperatures from the HadCRUT 5 database (Figures 13b, 13c, 13e, and 13f), which shows a 0.2–0.4°C increase in surface temperatures in the mid-latitude regions where the increase in lightning activity occurred.

9. Discussion

The results of this paper are based on frequency observations of the E_Z field component at NCK, Hungary which has realistic lightning source-observer configurations in the 90° nodal angular distance in the case of the first electric mode and in the ∼55° as well as the ∼40° nodal distances for the second and third modes (see Figure 1). Sátori and Zieger (1999) were the first to utilize the unique possibility of the nodal position of NCK with respect

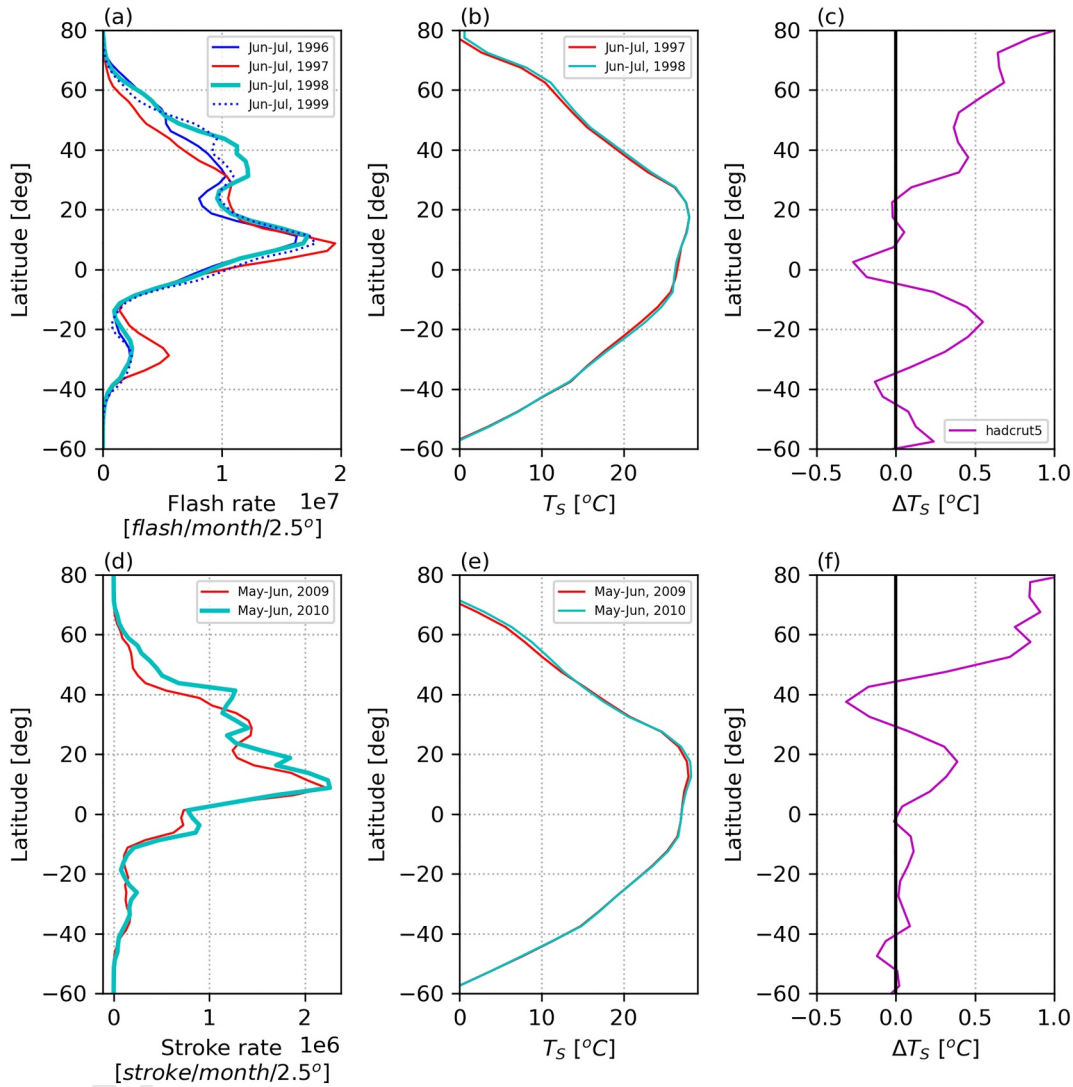

Figure 13. (a) Average meridional lightning distribution for the June–July months in 1996, 1997, 1998 and 1999, as observed by the Optical Transient Detector. (b) Average meridional lightning distribution for the May–June months in 2009 and 2010, as observed by the Word Wide Lightning Location Network. (b) and (e) show meridional surface temperature distributions (absolute temperatures) for the warm-to-cold transitions (turquoise curves) and the preceding warm periods (red curves), while (c) and (f) contain the difference of these curves (turquoise - red). The figure demonstrates that there is an increase in lightning activity at mid-latitudes following the sudden termination of the warm episodes, which may be related to the increase in surface temperature observed at these latitudes.

Table 1
The Centroid Latitude Positions of Global Lightning Activity and Centroid Weights (Total Flash Numbers) for the June–July Months in 1996, 1997, 1998, and 1999, as Observed by the Optical Transient Detector

	Centroid latitude	Centroid weight (total flash number)	ENSO condition
Jun–Jul 1996	18.21°N	2.670517e8	La Niña
Jun–Jul 1997	12.34°N	2.874031e8	El Niño
Jun–Jul 1998	19.10°N	2.989741e8	El Niño/La Niña transition
Jun–Jul 1999	17.56°N	2.971816e8	La Niña

to the sharp edge of African lightning activity at the southmost part of Sahara in the case of the third E_Z mode, and disclosed the meridional oscillation of global lightning activity on the ENSO time scale. The estimated magnitude of the meridional oscillation was about 4°–8° in angular distance. The underlying reason for this meridional oscillation was only given some years later by Trenberth et al. (2002). The thermal energy in the tropical belt absorbed in the warm phase of ENSO is released to extratropical regions in the warm-to-cold transition months. The energy is mainly transported to the NH due to the fact that these transitions usually occur in the early NH summer months. These atmosphere processes lead to extended and northward-shifted lightning activity shown here by the DFR and FL observations of the E_Z field component in the case of the warm-to-cold transition following the super El Nino event of 1997/1998 (Figure 12). Only the extension of the lightning area was observed for the smaller El Nino event of 2009/2010.

The first SR mode of the horizontal magnetic field does not have a nodal distance, its frequency monotonically increases from the source. Consequently, the magnetic field components can indicate large-scale distance variations of global lightning as it was demonstrated by Koloskov et al. (2020). Frequency changes associated with a few degrees of SOD changes are likely to be undetectable in the case of the first magnetic mode. Consequently, the presence of nodal distance/proximity can more efficiently be utilized to disclose SOD dependent changes of global/regional lightning with frequencies of the E_Z than with the frequencies of the horizontal magnetic field components. Additionally, the E_Z field component is responsive for the source position with respect to the observer in any direction while the responsiveness of magnetics depends on the coil orientation. Naturally, measuring the vertical electric (E_Z) and horizontal magnetic field components are not competitive SR observation methods, rather they can well complement each other. Recently, there is an increased number of SR stations (∼30–40) in the world measuring the horizontal magnetic field components (Bozóki et al., 2023). Multi-station SR measurements with well-calibrated magnetic records are available by now and are suitable to determine the charge moment change distribution of global lightning activity by SR inversion (see e.g., Prácser et al., 2019).

10. Conclusions

The position of the SR station at NCK in Central Europe has numerous lightning source-observer configurations (SOD) where and when the NCK observer gets in a nodal position with respect to the three main thunderstorm regions (Asia/MC, Africa, Americas) in the case of the first three modes of the vertical electric field component. The frequency sharply varies at the nodal lines in short SOD distances. Consequently, fine motions (<1 Mm) of global/regional lightning regions can be detected which has great importance from the point of view of climate change. We note that SR amplitude/intensity decrease in the nodal regions can rarely be detected.

Frequency variations of the E_Z field component related to nodal position of NCK:

- The annual mean frequency variation of the first E_Z mode is dominated by the annual northwest-southeast migration of the Asian/MC lightning region with respect to NCK.
- Semiannual frequency variations with April/October maxima appear in the case of the second E_Z mode. The highly variable frequencies from November to March indicate the nodal proximity of NCK with respect to the African lightning region in those months.
- Semiannual frequency variations with April/November minima in the hours of maximum lightning activity of Africa, and with March/October minima in the hours of maximum lightning activity of Asia/MC are visible in the case of the third E_Z mode. The 1 month shift between the minima of these two chimney regions hints at the difference in their seasonal migration dynamics. A NH spring-fall asymmetry (with a sharper spring transition compared to the fall season) can also be observed in both cases.
- The diurnal frequency pattern at NCK in January months was used to demonstrate how it is built up by the SOD-dependent frequency variations during the virtual zonal motion of the global lightning activity with maximum intensity in local afternoon.
- The high-resolution diurnal frequency patterns at NCK in six consecutive days of March 1996 with huge random-like frequency jumps indicate the nodal position of NCK with respect to Asia/MC and Central America in the hours of their maximum lightning activity. A SR amplitude/intensity decrease related to the nodal position was not observable.
- A squall-line formation of intense lightning activity in South America (Argentina) moving toward NCK in the early UT hours resulted in an extraordinary frequency excursion of the third E_Z mode at NCK around the nodal position of 90°. SR amplitude/intensity decrease was also observed for the common first and third nodal

distance in this case probably due to the lack of competitive lightning activity in those UT hours. The SOD variation during the frequency excursion was only ~300–400 km.

DFR and FL variations:

- The spread and northward-shifted lightning area shown by DFR and FL variations of the E_Z field component at NCK in the warm-cold transition of ENSO events were considered as the signature of thermal energy transfer to the extratropics with some-months delay after the formal El Niño phase in the tropics (Trenberth et al., 2002).

The E_Z record at NCK has about three-decade length and it is probably unique in the world especially with the high-quality peak frequency records. The analysis conducted by the authors demonstrated the potential of both using the NCK data set for identifying and tracking significant local events in nodal regions, such as squall-line formations associated with intense lightning activity, and for monitoring long-term interannual variations in lightning activity, for instance, those linked to ENSO episodes occurring over decadal timescales.

Data Availability Statement

The modeled and measured SR frequency data used in this study are available at a data repository (Sátori et al., 2024, https://doi.org/10.5281/zenodo.13220677). The v0.1 gridded satellite lightning data were produced by the NASA LIS/OTD Science Team (Principal Investigator, Dr. Hugh J. Christian, NASA/Marshall Space Flight Center) and are available from the Global Hydrology Resource Center (https://ghrc.nsstc.nasa.gov/home/). GLM data can be obtained through https://console.cloud.google.com/storage/browser/gcp-public-data-goes-16 (GOES-R, 2018). The HadCRUT5 analysis and the CRU climatology were downloaded from https://www.metoffice.gov.uk/hadobs/hadcrut5/data/HadCRUT.5.0.2.0/download.html and https://crudata.uea.ac.uk/cru/data/temperature, respectively.

Acknowledgments
The authors thank István Lemperger for his assistance in handling OTD data and József Bór for maintaining the SR measuring system at NCK. Karolina Szabóné André's efforts to produce a modern, python-based version of the complex demodulation algorithm is also highly appreciated. This work was supported by the National Research, Development, and Innovation Office, Hungary-NKFIH, project numbers K138824 (G.S., T.B., E.P.) and PD146019 (T.B.). The contribution of Earle Williams to this study was funded by the Hungarian Academy of Sciences as part of the Distinguished Guest Scientists Fellowship Programme (VK-6/2023). The contribution of Earle Williams was supported by a grant from the US National Science Foundation (Grant AGS-1945871, "The GlobalCircuits Paradox"). The authors wish to thank the World Wide Lightning Location Network (http://wwlln.net), a collaboration among over 50 universities and institutions, for providing the lightning location data used in this study.

References

Ahmad, A., & Ghosh, M. (2017). Variability of lightning activity over India on ENSO time scales. *Advances in Space Research*, *60*(11), 2379–2388. https://doi.org/10.1016/j.asr.2017.09.018

Balser, M., & Wagner, C. A. (1960). Observation of Earth-ionosphere cavity resonances. *Nature*, *188*(4751), 638–641. https://doi.org/10.1038/188638a0

Banks, R. J. (1975). Complex demodulation of geomagnetic data and the estimation of transfer functions. *Geophysical Journal International*, *43*(1), 87–101. https://doi.org/10.1111/j.1365-246X.1975.tb00629.x

Beamish, D., Hanson, H. W., & Webb, D. C. (1979). Complex demodulation applied to Pi2 geomagnetic pulsations. *Geophysical Journal International*, *58*(2), 471–493. https://doi.org/10.1111/j.1365-246X.1979.tb01035.x

Blakeslee, R. J., Mach, D. M., Bateman, M. G., & Bailey, J. C. (2014). Seasonal variations in the lightning diurnal cycle and implications for the global electric circuit. *Atmospheric Research*, *135–136*, 228–243. https://doi.org/10.1016/j.atmosres.2012.09.023

Bliokh, P. V., Nickolaenko, A. P., Filippov, Yu.F., & Jones, D. L. (Eds.). (1980). *Schumann resonances in the Earth-ionosphere cavity*. Peter Peregrinus Ltd.

Boldi, R., Williams, E., & Guha, A. (2017). Determination of the global-average charge moment of a lightning flash using Schumann resonances and the LIS/OTD lightning data. *Journal of Geophysical Research: Atmosphere*, *123*(1), 108–123. https://doi.org/10.1002/2017JD027050

Bozóki, T., Prácser, E., Sátori, G., Dálya, G., Kapás, K., & Takátsy, J. (2019). Modeling Schumann resonances with schupy. *Journal of Atmospheric and Solar-Terrestrial Physics*, *196*, 105144. https://doi.org/10.1016/j.jastp.2019.105144

Bozóki, T., Sátori, G., Williams, E., Guha, A., Liu, Y., Steinbach, P., et al. (2023). Day-to-day quantification of changes in global lightning activity based on Schumann resonances. *Journal of Geophysical Research: Atmospheres*, *128*(11), e2023JD038557. https://doi.org/10.1029/2023JD038557

Christian, H. J., Blakeslee, R. J., Boccippio, D. J., Boeck, W. L., Buechler, D. E., Driscoll, K. T., et al. (2003). Global frequency and distribution of lightning as observed from space by the optical transient detector. *Journal of Geophysical Research*, *108*(D1), ACL4-1–ACL4-15. https://doi.org/10.1029/2002JD002347

Chronis, T. G., Goodman, S. J., Cecil, D., Buechler, D., Robertson, F. J., Pittman, J., & Blakeslee, R. J. (2008). Global lightning activity from the ENSO perspective. *Geophysical Research Letters*, *35*(19). https://doi.org/10.1029/2008GL034321

Clark, A. G., & Cecil, D. J. (2024). Interannual lightning variability within the TRMM LIS dataset using an ENSO perspective. *Monthly Weather Review*, *152*(4), 987–1005. https://doi.org/10.1175/MWR-D-23-0115.1

Cohen, J. C. P., Silva Dias, M. A. F., & Nobre, C. A. (1995). Environmental conditions associated with Amazonian squall lines: A case study. *Monthly Weather Review*, *123*(11), 3163–3174. https://doi.org/10.1175/1520-0493(1995)123<3163:ECAWAS>2.0.CO;2

Erdelyi, A. (1953). *Higher transcendental functions*. McGraw-Hill.

Füllekrug, M. (2021). Simulation of Earth-ionosphere cavity resonances with lightning flashes reported by OTD/LIS. *Journal of Geophysical Research: Atmospheres*, *126*(24), e2021JD035721. https://doi.org/10.1029/2021JD035721

Galejs, J. (1970). Frequency variations of Schumann resonances. *Journal of Geophysical Research*, *75*(16), 3237–3251. https://doi.org/10.1029/JA075i016p03237

Galejs, J. (1972). *Terrestrial propagation of long electromagnetic waves*. Pergamon Press.

Garstang, M., Massie, H. L., Jr., Halverson, J., Greco, S., & Scala, J. (1994). Amazon coastal squall lines. Part I: Structure and kinematics. *Monthly Weather Review*, *122*(4), 608–622. https://doi.org/10.1175/1520-0493(1994)122<0608:ACSLPI>2.0.CO;2

GOES-R Algorithm Working Group and GOES-R Series Program. (2018). NOAA GOES-R series geostationary lightning mapper (GLM) level 2 lightning detection: Events, Groups, and flashes [Dataset]. NOAA National Centers for Environmental Information. https://doi.org/10.7289/V5KH0KK6

Goodman, S. J., Blakeslee, R. J., Koshak, W. J., Mach, D., Bailey, J., Buechler, D., et al. (2013). The GOES-R Geostationary Lightning Mapper (GLM). *Atmospheric Research*, *125*(126), 34–49. https://doi.org/10.1016/j.atmosres.2013.01.006

Goodman, S. J., Buechler, D. E., Knupp, K., Driscoll, K. T., & McCaul, E. W. (2000). The 1997–1998 El Niño event and related wintertime lightning variations in the Southeastern United States. *Geophysical Research Letters*, *27*(4), 541–544. https://doi.org/10.1029/1999GL010808

Hamid, E. F., Kawasaki, Z. I., & Mardiana, R. (2001). Impact of the 1997-98 El Niño event on lightning activity over Indonesia. *Geophysical Research Letters*, *28*(1), 147–150. https://doi.org/10.1029/2000GL011374

Hobara, Y., Hayakawa, M., Williams, E., Boldi, R., & Downe, E. (2006). Electrical properties of sprite-producing lightning deduced from a single ELF field site. In M. Füllekrug, E. A. Mareev, & M. J. Rycroft (Eds.), *Sprites, elves and intense lightning discharges*, *NATO Sci. Ser. Ser. II* (Vol. 225, pp. 211–235). Springer.

Hutchins, M. L., Holzworth, R. H., Brundell, J. B., & Rodger, C. J. (2012). Relative detection efficiency of the world wide lightning location network. *Radio Science*, *47*(6), RS6005. https://doi.org/10.1029/2012RS005049

Jones, D. L. (1969). The apparent resonance frequencies of the Earth-ionosphere cavity when excited by a single dipole source. *Journal of Geomagnetism and Geoelectricity*, *21*(3), 679–684. https://doi.org/10.5636/jgg.21.679

Jones, P. D., New, M., Parker, D. E., Martin, S., & Rigor, I. G. (1999). Surface air temperature and its changes over the past 150 years. *Review of Geophysics*, *37*(2), 173–199. https://doi.org/10.1029/1999RG900002

Kemp, D. T. (1971). The global radio-location of large lightning discharges from single station observations of ELF disturbances in the Earth-ionosphere waveguide. *Journal of Atmospheric and Terrestrial Physics*, *33*, 919–928. https://doi.org/10.1016/0021-9169(71)90091-2

Koloskov, A. V., Nickolaenko, A. P., Yampolsky, Y. M., Yu, C., Budanov, O. V., & Budanov, O. V. (2020). Variations of global thunderstorm activity derived from the long-term Schumann resonance monitoring in the Antarctic and in the Arctic. *Journal of Atmospheric and Solar-Terrestrial Physics*, *201*, 105231. https://doi.org/10.1016/j.jastp.2020.105231

Koloskov, O. V., Nickolaenko, A. P., Yampolsky, Y. M., & Budanov, O. V. (2022). Electromagnetic seasons in Schumann resonance records. *Journal of Geophysical Research: Atmospheres*, *127*(17). https://doi.org/10.1029/2022JD036582

Kousky, V. E. (1980). Diurnal rainfall variation in northeast Brazil. *Monthly Weather Review*, *108*(4), 488–498. https://doi.org/10.1175/1520-0493(1980)108<0488:DRVINB>2.0.CO;2

Kulak, A., Mlynarczyk, J., Zieba, S., Micek, S., & Nieckarz, Z. (2006). Studies of ELF propagation in the spherical shell cavity using a field decomposition method based on asymmetry of Schumann resonance curves. *Journal of Geophysical Research*, *111*(A10). https://doi.org/10.1029/2005JA011429

Kulkarni, M. K., Revadekar, J. V., Verikoden, H., & Athale, S. (2015). Thunderstorm days and lightning activity in association with El Nino. *Vayu Mandal*, *41*, 39–43.

Kulkarni, M. N., & Siingh, D. (2014). The relation between lightning and cosmic rays during ENSO with and without IOD—A statistical study. *Atmospheric Research*, *143*, 129–141. https://doi.org/10.1016/j.atmosres.2014.02.010

Kumar, P. R., & Kamra, A. K. (2012). Variability of lightning activity in south/southeast Asia during 1997–98 and 2002–03 El Nino/La Nina events. *Atmospheric Research*, *118*, 84–102. https://doi.org/10.1016/j.atmosres.2012.06.004

Ludlam, F. H. (1980). *Clouds and storms: The behavior and effect of water in the atmosphere*. Pennsylvania State University Press.

Madden, T., & Thompson, W. (1965). Low-frequency electromagnetic oscillation of the Earth-ionosphere cavity. *Review of Geophysics*, *3*(2), 211–254. https://doi.org/10.1029/RG003i002p00211

Morice, C. P., Kennedy, J. J., Rayner, N. A., Winn, J. P., Hogan, E., Killick, R. E., et al. (2021). An updated assessment of near-surface temperature change from 1850: The HadCRUT5 data set. *Journal of Geophysical Research: Atmospheres*, *126*(3), e2019JD032361. https://doi.org/10.1029/2019JD032361

Mushtak, V. C., & Williams, E. R. (2002). ELF propagation parameters for uniform models of the Earth-ionosphere waveguide. *Journal of Atmospheric and Solar-Terrestrial Physics*, *64*(18), 1989–2001. https://doi.org/10.1016/S1364-6826(02)00222-5

Nelson, P. H. (1967). *Ionospheric perturbations and Schumann resonance data*. Project NR-371-401 (PhD dissertation). Geophysics Laboratory, Massachusetts Institute of Technology.

Nickolaenko, A. P. (2015a). Monitoring the peak frequency of Schumann resonance and analemma. *Telecommunications and Radio Engineering*, *74*(9), 815–824. https://doi.org/10.1615/TelecomRadEng.v74.i9.70

Nickolaenko, A. P. (2015b). Deducing parameters of the world thunderstorms from the Schumann resonance records. *Telecommunications and Radio Engineering*, *74*(2), 147–161. https://doi.org/10.1615/TelecomRadEng.v74.i2.40

Nickolaenko, A. P., & Hayakawa, M. (2002). *Resonances in the Earth–ionosphere cavity*. Springer.

Nickolaenko, A. P., Koloskov, A. V., Hayakawa, M., Yampolski, Y. M., Budanov, V. E., & Korepanov, V. E. (2015). 11-year solar cycle in Schumann resonance data as observed in Antarctica. *Sun and Geosphere*, *10*(1), 39–49.

Nickolaenko, A. P., & Rabinowicz, L. M. (1995). Study of annual changes of global lightning distribution and frequency variations of the first Schumann resonance mode. *Journal of Atmospheric and Solar-Terrestrial Physics*, *57*(11), 1345–1348. https://doi.org/10.1016/0021-9169(94)00114-4

Nickolaenko, A. P., Sátori, G., Zieger, B., Rabinowicz, L. M., & Kudintseva, I. G. (1998). Parameters of global thunderstorm activity deduced from the long-term Schumann resonance records. *Journal of Atmospheric and Solar-Terrestrial Physics*, *60*(3), 387–399. https://doi.org/10.1016/S1364-6826(97)00121-1

Ogawa, T., Tanaka, Y., & Yasuhara, M. (1968). Schumann resonance and worldwide thunderstorm activity. *Journal of Geomagnetism and Geoelectricity*, *21*(1), 447–452. https://doi.org/10.5636/jgg.21.447

Ondrášková, A., Kostecký, P., Ševčík, S., & Rosenberg, L. (2007). Long-term observations of Schumann resonances at Modra Observatory. *Radio Science*, *42*(2). https://doi.org/10.1029/2006RS003478

Polk, C. (1969). Relation of ELF noise and Schumann resonances to thunderstorm activity. In H. Volland (Ed.), *Planetary electrodynamics*. CRC Press.

Prácser, E., Bozóki, T., Sátori, G., Williams, E., Guha, A., & Yu, H. (2019). Reconstruction of global lightning activity based on Schumann resonance measurements: Model description and synthetic tests. *Radio Science*, *54*(3), 254–267. https://doi.org/10.1029/2018RS006772

Sahu, R. K., Choudhury, G., Vissa, N. K., Tyagi, B., & Nayak, S. (2022). The impact of El-Niño and La-Niña on the pre-monsoon convective systems over eastern India. *Atmosphere*, *13*(8), 1261. https://doi.org/10.3390/atmos13081261

Sátori, G. (1996). Monitoring Schumann resonances-II. Daily and seasonal frequency variations. *Journal of Atmospheric and Terrestrial Physics*, *58*(13), 1483–1488. https://doi.org/10.1016/0021-9169(95)00146-8

Sátori, G., Bozóki, T., & Prácser, E. (2024). Modeled and measured SR frequency data (Ez, NCK, Hungary) (2.0) [Dataset]. *Zenodo*. https://doi.org/10.5281/zenodo.13220677

Sátori, G., Mushtak, V., & Williams, E. (2009). Schumann resonance signatures of global lightning activity. In H. D. Betz, U. Schumann, & P. Laroche (Eds.), *Lightning: Principles, instruments and applications*. Springer. https://doi.org/10.1007/978-1-4020-9079-0_16

Sátori, G., Rycroft, M., Bencze, P., Märcz, F., Bór, J., Barta, V., et al. (2013). An overview of thunderstorm-related research on the atmospheric electric field, Schumann resonances, sprites, and the ionosphere at Sopron, Hungary. *Surveys in Geophysics*, *34*(3), 255–292. https://doi.org/10.1007/s10712-013-9222-6

Sátori, G., Szendrői, J., & Verő, J. (1996). Monitoring Schumann resonances—I. Methodology. *Journal of Atmospheric and Terrestrial Physics*, *58*(13), 1475–1481. https://doi.org/10.1016/0021-9169(95)00145-X

Sátori, G., Williams, E., & Lemperger, I. (2009). Variability of global lightning activity on the ENSO time scale. *Atmospheric Research*, *91*(2–4), 500–507. https://doi.org/10.1016/j.atmosres.2008.06.014

Sátori, G., Williams, E., & Mushtak, V. (2005). Response of the Earth-ionosphere cavity resonator to the 11-year solar cycle in X-radiation. *Journal of Atmospheric and Solar-Terrestrial Physics*, *67*(6), 553–562. https://doi.org/10.1016/j.jastp.2004.12.006

Sátori, G., & Zieger, B. (1999). El Niño related meridional oscillation of global lightning activity. *Geophysical Research Letters*, *26*(10), 1365–1368. https://doi.org/10.1029/1999GL900264

Sátori, G., & Zieger, B. (2003). Areal variations of the worldwide thunderstorm activity on different time scales as shown by Schumann resonances. In S. Chauzy & P. Laroche (Eds.), *Proceeding of the 12th ICAE, global lightning and climate* (pp. 765–768).

Schumann, W. O. (1952). Über die strahlungslosen Eigenschwingungen einer leitenden Kugel, die von einer Luftschicht und einer Ionosphärenhülle umgeben ist. *Zeitschrift für Naturforschung*, *7*(2), 149–154. https://doi.org/10.1515/zna-1952-0202

Sentman, D. D. (1996). Schumann resonance spectra in two-scale-height Earth-ionosphere cavity. *Journal of Geophysical Research*, *101*(D5), 9479–9487. https://doi.org/10.1029/95JD03301

Tinmaker, M. I. R., Aslam, M. Y., Ghude, S. D., & Chate, D. M. (2017). Lightning activity with rainfall during El Nino and La Nina events over India. *Theoretical and Applied Climatology*, *130*(1–2), 391–400. https://doi.org/10.1007/s00704-016-1883-x

Trenberth, K. E., Caron, J. M., Stepaniak, D. P., & Worley, S. (2002). Evolution of El Niño-Southern oscillation and global surface temperatures. *Journal of Geophysical Research*, *107*(D8), 4065. https://doi.org/10.1029/2000JD000298

Wait, J. R. (1996). *Electromagnetic waves in stratified media*. IEEE Press.

Williams, E., Bozóki, T., Sátori, G., Price, C., Steinbach, P., Guha, A., et al. (2021). Evolution of global lightning in the transition from cold to warm phase preceding two super El Niño events. *Journal of Geophysical Research: Atmospheres*, *126*(3), e2020JD033526. https://doi.org/10.1029/2020JD033526

Williams, E. R. (1992). The Schumann resonance: A global tropical thermometer. *Science*, *256*(5060), 1184–1187. https://doi.org/10.1126/science.256.5060.1184